Supplemental Material

Research Article

Vandetanib Reduces Inflammatory Cytokines and Ameliorates COVID-19 in Infected Mice

Ana C. Puhl[1][*][#], Giovanni F. Gomes[2][*], Samara Damasceno[2], Ethan J. Fritch[3], James A. Levi[4], Nicole J. Johnson[4], Frank Scholle[4], Lakshmanane Premkumar[3], Brett L. Hurst[5,6], Felipe LeeMontiel[7], Flavio P. Veras[2], Sabrina S. Batah[8], Alexandre T. Fabro[8], Nathaniel J. Moorman[3,9,10], Boyd L. Yount[11], Rebekah Dickmander[3,9,10], Ralph Baric[3,9,11], Kenneth H. Pearce[10,12], Fernando Q. Cunha[2], José C. Alves-Filho[2][#], Thiago M. Cunha[2][#] and Sean Ekins[1][#].

[1]Collaborations Pharmaceuticals, Inc., 840 Main Campus Drive, Lab 3510, Raleigh, NC 27606, USA.

[2]Center for Research in Inflammatory Diseases (CRID), Ribeirao Preto Medical School, University of Sao Paulo, Avenida Bandeirantes, 3900, Ribeirao Preto, 14049-900 ; Sao Paulo, Brazil.

[3]Department of Microbiology and Immunology, University of North Carolina School of Medicine, Chapel Hill NC 27599, USA.

[4]Department of Biological Sciences, North Carolina State University, Raleigh, NC, USA.

[5]Institute for Antiviral Research, Utah State University, Logan, UT, USA.

[6]Department of Animal, Dairy and Veterinary Sciences, Utah State University, Logan, UT, USA.

[7]PhenoVista Biosciences, 6195 Cornerstone Ct E. #114 San Diego CA 92121.

[8]Department of Pathology and Legal Medicine, Ribeirão Preto Medical School, University of São Paulo, Ribeirão Preto, Brazil.

[9]Rapidly Emerging Antiviral Drug Discovery Initiative, University of North Carolina at Chapel Hill, Chapel Hill, NC, USA.

[10]Center for Integrative Chemical Biology and Drug Discovery, Chemical Biology and Medicinal Chemistry, Eshelman School of Pharmacy, University of North Carolina, Chapel Hill, North Carolina 27599, USA.

[11]Department of Epidemiology, Gillings School of Public Health, University of North Carolina at Chapel Hill, Chapel Hill, NC, USA.

29

[12]UNC Lineberger Comprehensive Cancer Center, Chapel Hill, North Carolina 27599, USA.

[*]Both authors contributed equally

[#]To whom correspondence should be addressed: Ana C. Puhl, E-mail address: ana@collaborationspharma.com; Sean Ekins, E-mail address: sean@collaborationspharma.com; Thiago M Cunha E-mail address: thicunha@fmrp.usp.br

Supplemental Materials

METHODS

Chemicals and reagents

Entrectinib, Vandetanib were purchased from MedChemExpress (MCE, Monmouth Junction, NJ).

Expression and purification of Spike RBD of SARS-CoV-2

A codon-optimized gene encoding for SARS-CoV-2 (331 to 528 amino acids, QIS60558.1) was expressed in Expi293 cells (Thermo Fisher Scientific) with human serum albumin secretion signal sequence and fusion tags (6xHistidine tag, Halo tag, and TwinStrep tag) as described before [1]. S1 RBD was purified from the culture supernatant by nickel–nitrilotriacetic acid agarose (Qiagen), and purity was confirmed to by >95% as judged by coomassie stained SDS-PAGE. The purified RBD protein was buffer exchanged to 1x PBS prior to analysis by Microscale Thermophoresis.

Microscale Thermophoresis

We used Microscale thermophoresis (MST) to detect binding of entrectinib to the Spike RBD protein. The experiments were performed according to the manufacturer's instructions (NanoTemper) and as described previously [2]. Briefly, for protein labeling, 6 µM of protein was be used with 3-fold excess NHS dye in MST Buffer (HEPES 10 mM pH 7.4, NaCl 150 mM), using Monolith Protein Labeling Kit RED-NHS 2nd Generation

31

(Amine Reactive). Free dye was removed, and protein eluted in MST buffer, and centrifuged at 15 k rcf for 10 min. Binding affinity measurements were determined using NanoTemper's Monolith NT.115 Pico (Nanotemper) and were performed using 5 nM protein a serial dilution of compounds, starting at 100 µM in MST buffer containing 5 % glycerol, 1 mM β-Mercaptoethanol and 0.1 % Triton X-100. Spike RBD was incubated at room temperature in presence of compounds for 20 min prior measurement. Samples were then loaded into sixteen standard capillaries (NanoTemper Technologies) and fluorescence was recorded for 20 s using 20 % laser power and 40 % MST power. The temperature of the instrument was set to 23°C for all measurements. After recording the MST time traces, data were analysed. K_D value was calculated from ligand concentration-dependent changes in the fraction bound (F_{bound}) of Dye-Spike RBD after 10 s of thermophoresis. The assay was performed in quadruplicate and the values reported were generated through the usage of MO Affinity Analysis software (NanoTemper Technologies).

Pseudovirus Assay

Cell imaging and analysis was conducted at Phenovista Biosciences. HUVEC single cell donor (Lonza, cat#C2517A) cells were transduced at room temperature with ACE2 using a BacMam viral vector at a concentration of $2e^9$ VG/ml (Montana Molecular #C1120G Pseudo SARS-CoV-2 D614G Green Reporter) followed by incubation at 36°C for 24 hours. After this step, inhibitor compounds were diluted to 1µM and incubated for 60 minutes with 2e9 VG/ml of Pseudo SARS-CoV2 or Pseudo SARS-CoV2 D614G

baculovirus (Montana Molecular #C1110G, #C1120G). Prior to fixation with PFA, cell nuclei were stained with Hoechst, and images were acquired with the high content screening InCell Analyzer HS6500 microscope (20X Magnification). Quantitative analysis was done with ThermoFisher HCS Studio Cell analysis suite.

SARS-Cov-2 tested in A549-ACE2 cells

A549-ACE2 cells were plated in Corning black walled clear bottom 96 well plates 24 hours before infection for confluency. Drug stocks were diluted in DMSO for a 200X concentration in an 8-point 1:4 dilution series. Prepared 200X dilutions were then diluted to 2X concentration in infection media (Gibco DMEM supplemented with 5% HyClone FetalCloneII, 1% Gibco NEAA, 1% Gibco Pen-Strep). Growth media was removed, and cells were pretreated with 2 X drug for 1 hour prior to infection at 37C and 5% CO2. Cells were either infected at a MOI of 0.02 with infectious clone SARS-CoV-2-nLuc [3] or mock infected with infection media to evaluate toxicity. 48 hours post infection wells were treated with Nano-Glo Luciferase assay activity to measure viral growth or CytoTox-Glo Cytotoxicity assay to evaluate toxicity of drug treatments, performed per manufacturer instructions (Promega). Nano-Glo assays were read using a Molecular Devices SpectraMax plate reader and CytoTox-Glo assays were read using a Promega GloMax plate reader. Vehicle treated wells on each plate were used to normalize replication and toxicity. Drug treatment was performed in technical duplicate and biological triplicate.

SARS-Cov-2 tested in Calu-3 cells

Calu-3 (ATCC, HTB-55) cells were pretreated with test compounds for 2 hours prior to continuous infection with SARS-CoV-2 (isolate USA WA1/2020) at a MOI=0.5. Forty-eight hours post-infection, cells were fixed, immunostained, and imaged by automated microscopy for infection (dsRNA+ cells/total cell number) and cell number. Sample well data was normalized to aggregated DMSO control wells and plotted versus drug concentration to determine the IC_{50} (infection: blue) and CC_{50} (toxicity: green).

SARS-Cov-2 tested in Caco-2 cells

For the Caco-2 VYR assay, the methodology is identical to the Vero 76 cell assay other than the insufficient CPE is observed on Caco-2 cells to allow EC50 calculations. Supernatant from the Caco-2 cells are collected on day 3 post-infection and titrated on Vero 76 cells for virus titer as before.

Murine Hepatitis Virus

Each compound was tested for antiviral activity against murine hepatitis virus (MHV), a group 2a betacoronavirus, in DBT cells. MHV-A59 with nano-Luciferase: The MHV-A59 G plasmid was engineered to replace most of the coding sequence for orf4a and 4b with nano-luciferase (nLuc). Briefly, nucleotides 27,983 to 28,267 were removed and replaced with SalI and SacII restriction sites; approximately 111 bp of the 3' end of orf4B was left to maintain the TRS for orf5. Nano-luciferase was pcr amplified with primers 5'nLuc SalI (5'-NNNNNNGTCGACATGGTCTTCACACTCGAAGATTTC-3') and

34

3'nLuc SacII (5'-NNNNNNCCGCGGTTACGCCAGAATGCGTTCGCAC-3'), digested with SalI and SacII and then cloned into the G plasmid which had been similarly digested. A sequence verified G-nLuc plasmid was used with MHV-A59 wild type A, B, C, D, E and F plasmids to recover virus expressing nLuc, using our previously described molecule clone (Systematic assembly of a full-length infectious cDNA of mouse hepatitis virus strain A59 [4]. Each compound was tested against MHV using an 8-point dose response curve consisting of serial fourfold dilutions, starting at 10 µM. The same range of compound concentrations was also tested for cytotoxicity in uninfected cells.

HCoV 229E antiviral assay

HCoV 229E, (a gift from Ralph Baric, UNC, Chapel Hill) was propagated on Huh-7 cells and titers were determined by $TCID_{50}$ assay on Huh-7 cells. Huh-7 cells were plated at a density of 25,000 cells per well in 96 well plates and incubated for 24 h at 37°C and 5% CO_2. Growth media was removed, and cells were pretreated with 2 X drug for 1 hour prior to infection at 37C and 5% CO2. Cells were infected with HCoV 229E at a MOI of 0.1 in a volume of 50 ul MEM 1+1+1 (Modified Eagles Medium, 1% FBS, 1% antibiotics, 1% HEPES buffer) for 1 hour. Virus was removed, cells rinsed once with PBS growth medium was added back at a volume of 100 µl. Supernatants were harvested after 24 h, serially ten-fold diluted, and virus titer was determined by $TCID_{50}$ assay on Huh-7 cells. CPE was monitored by visual inspection at 96h post infection. $TCID_{50}$ titers were calculated using the Spearmann-Karber method [5, 6].

Mouse studies

Ethical approval

All the experimental procedures were performed in accordance with the guide for the use of laboratory animals of the University of Sao Paulo and approved by the institutional ethics committee under the protocol number 105/2021.

SARS-CoV-2

SARS-CoV-2 was isolated from a COVID-19 positive-tested patient. The virus was propagated and titrated in Vero E6 cells in a biosafety level 3 laboratory (BSL3) at the Ribeirao Preto Medical school (Ribeirao Preto, Brazil). Cells were cultured in DMEM medium supplemented with 10% fetal bovine serum (FBS) and antibiotic/antimycotic (Penicillin 10,000 U/mL; Streptomycin10,000 µg/mL). The viral inoculum was added to Vero cells in DMEM (FBS 2%) incubated at 37 °C with 5% CO_2 for 48 h. The cytopathogenic effect was observed under a microscope. Cell monolayer was collected, and the supernatant was stored in -70 ºC. Virus titration was made by the plaque-forming units (PFU).

K18-hACE2 mice

To evaluate the effects of vandetanib *in vivo*, we infected the K18-hACE2 humanized mice (B6.Cg-Tg(K18-ACE2)2Prlmn/J)[7, 8, 9]. K18-hACE2 mice were obtained from The Jackson Laboratory and were breed in the Centro de Criação de Animais Especiais (Ribeirão Preto Medical School/University of São Paulo). This mouse has been used as model for SARS-CoV-2-induced disease and it presents clinical signs, and biochemical and histopathological changes compatible with the human disease[8, 9,]

36

[10, 11, 12, 13, 14]. Mice had access to water and food *ad libitum*. For the experimental infection, animals were transferred to the BSL2 facility.

SARS-CoV-2 experimental infection and treatments

Female K18-hACE2 mice, aged 8 weeks, were infected with $2x10^4$ PFU of SARS-CoV-2 (in 40 μL) by intranasal route. Uninfected mice were inoculated with equal volume of PBS. On the day of infection, 1 h before virus inoculation, animals were treated with vandetanib (25 mg/kg, i.p.) (n = 6). Five infected animals remained untreated. Vandetanib was also given once daily on the days 1, 2 and 3 post-infection. Body weight was evaluated on the baseline and on all the days post-infection. On the day 3 post-infection, 6 h after treatments, animals were humanely euthanized, and lungs were collected. Right lung was collected, harvested, and homogenized in PBS with steel glass beads. The homogenate was added to TRIzol reagent (1:1), for posterior viral titration via RT-qPCR, or to lysis buffer (1:1), for ELISA assay, and stored at -70 °C. The left lung was collected in paraformaldehyde (PFA 4%) for posterior histological assessment.

Absolute viral copies quantification

Total RNA from the lung was obtained using the Trizol® (Invitrogen, CA, EUA) method and quantified using NanoDrop One/Onec (ThermoFisher Scientific, USA). A total of 800 ng of RNA was used to synthesize cDNA. cDNA was synthesized using the High-Capacity cDNA Reverse Transcription kit (Applied Biosystems, Foster City, CA, USA), following the manufacturer's protocol. The determination of the absolute number

37

of viral copies was made by a taqman real-time qPCR assay with the ad of the StepOneTM Real-Time PCR System (Applied Biosystems, Foster City, CA, USA). A standard curve was generated in order to obtain the exact number of copies in the tested sample. The standard curve was performed using an amplicon containing 944 bp cloned from a plasmid (PTZ57R/T CloneJetTM Cloning Kit Thermo Fisher®), starting in the nucleotide 14 of the gene N. To quantify the number of copies, a serial dilution of the plasmid in the proportion of 1:10 was performed. Commercial primers and probes for the N1 gene and RNAse P (endogenous control) were used for the quantification (2019-nCov CDC EUA Kit, IDT), following the CDC's instructions.

ELISA assay

Lung homogenate was added to RIPA buffer in proportion of 1:1, and then centrifuged at 10,000 g at 4 °C for 10 minutes. Supernatant was collected and stored in -70 °C until use. The Sandwich ELISA method was performed to detect the concentration cytokines and chemokines using kits from R&D Systems (DuoSet), according to the manufacturer. The following targets were evaluated: IL-6, IL-10, IL-1β, TNF-α, INF-1β, CCL2, CCL3, CCL4, CXCL1, CXCL2, and CXCL10.

Lung histopathological process and analyses

Five micrometer lung slices were submitted to Hematoxylin and Eosin staining. A total of 10 photomicrographs in 40X magnification per animal were randomly obtained using a microscope Novel (Novel L3000 LED, China) coupled to a HDI camera for images capture. The total septal area and total area were analyzed with the aid of the

Pro Plus 7 software (Media Cybernetics, Inc., MD, USA). Morphometric analysis was performed in accordance with the protocol established by the American Thoracic Society and European Thoracic Society (ATS/ERS) [15].

Figure S1: *In vitro* antiviral SARS-CoV-2 testing in Calu-3 cells. Calu-3 (ATCC, HTB-55) cells were pretreated with test compounds for 2 hours prior to continuous infection with SARS-CoV-2 (isolate USA WA1/2020) at a MOI=0.5. Forty-eight hours post-infection, cells were fixed, immunostained, and imaged by automated microscopy for infection (dsRNA+ cells/total cell number) and cell number. Sample well data was normalized to aggregated DMSO control wells and plotted versus drug concentration to determine the IC_{50} (infection: blue) and CC_{50} (toxicity: green). Percentage of Control (POC)=(sample well measurement /aggregated DMSO avg)*100 for n=3 replicates. **A)** remdesivir, **B)** entrectinib.
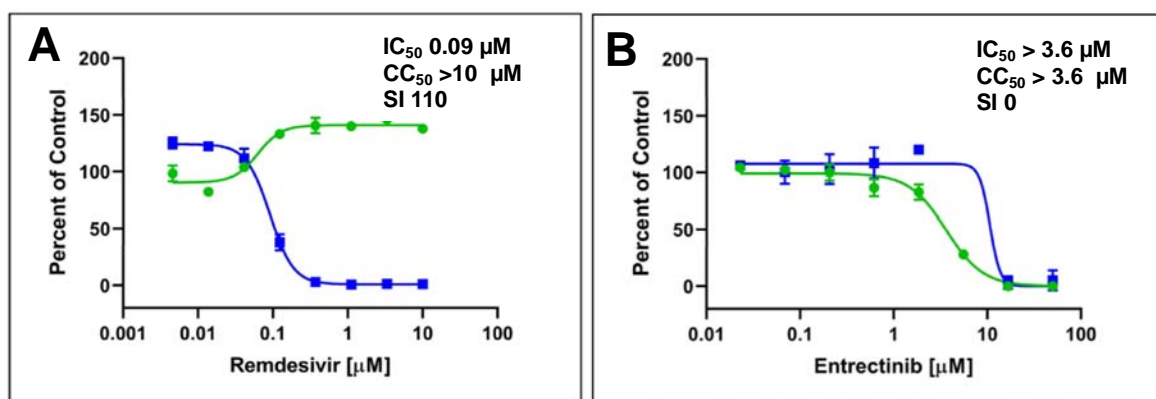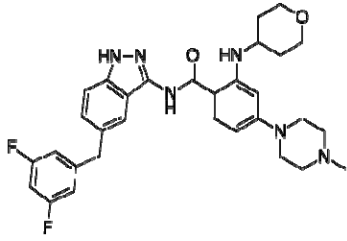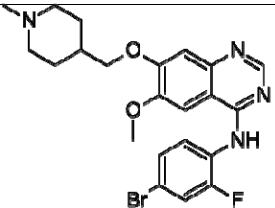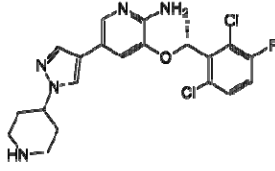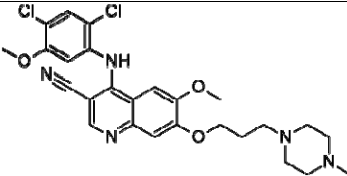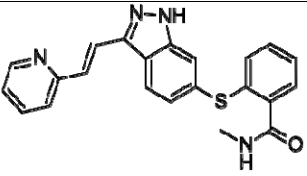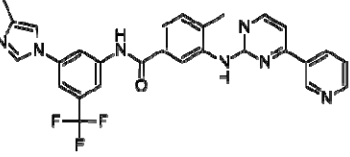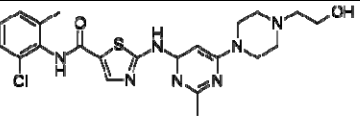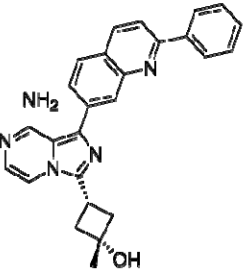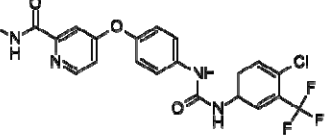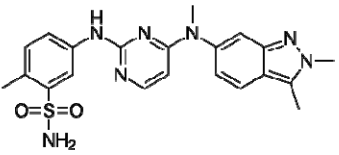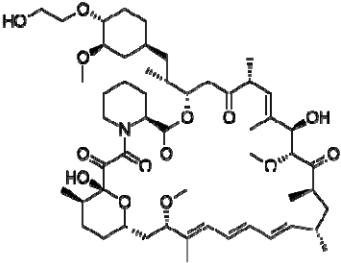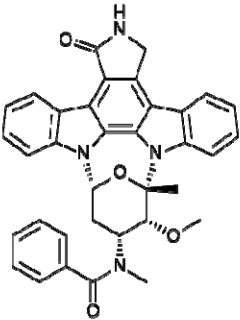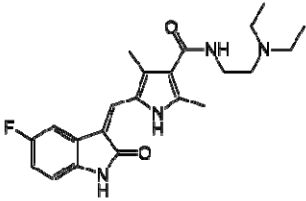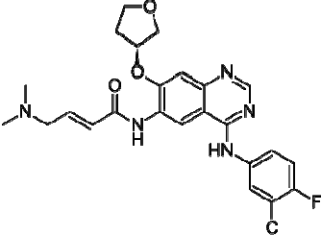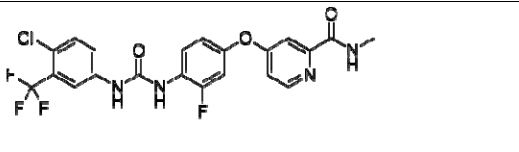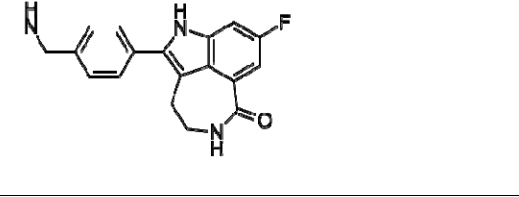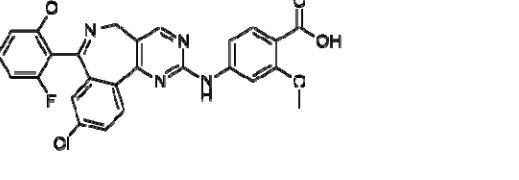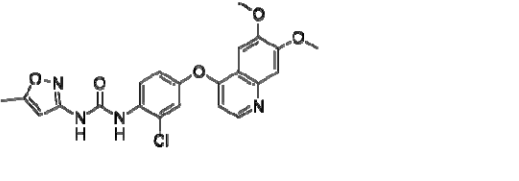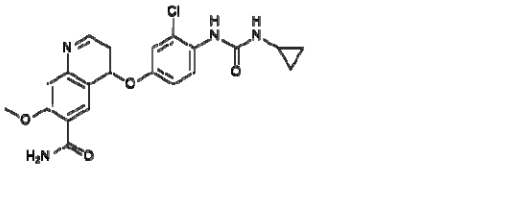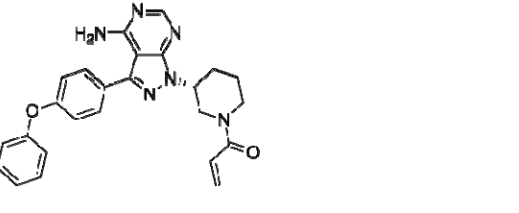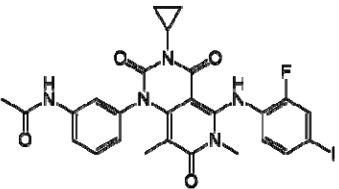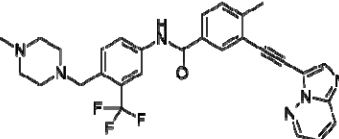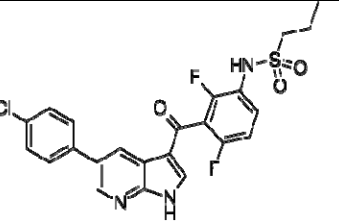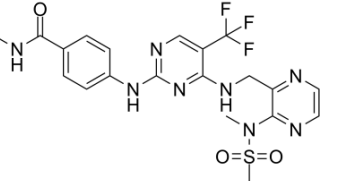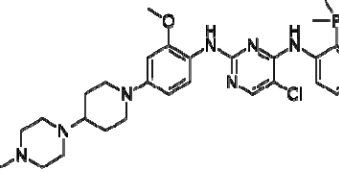
Table S1. Kinase inhibitors tested against MHV and SARS-CoV-2.

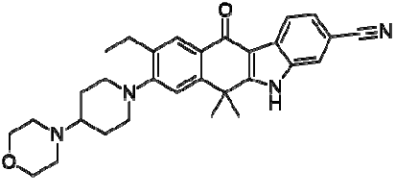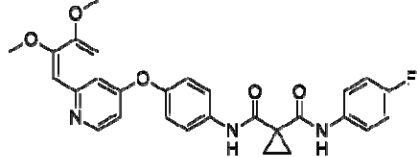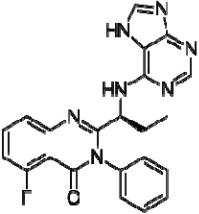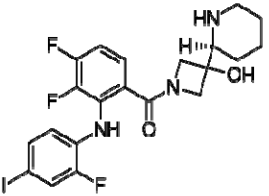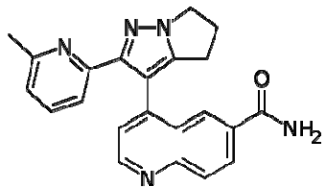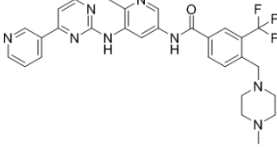| Compound	Structure	Target	% Inhibition MHV- dbt cells at 10 μM	A549-ACE2 SARS-CoV-2	Caco-2	Calu-3	HCOV
Entrectinib		Selective tyrosine kinase inhibitor (TKI), of the tropomyosin receptor kinases (TRK) A, B and C, C-ros oncogene 1 (ROS1) and anaplastic lymphoma kinase (ALK)	97	1.97 μM	N	toxic	Y
Vandetanib		Inhibitor of vascular endothelial growth factor receptor-2, epidermal growth factor receptor, and RET tyrosine kinases. RET tyrosine kinases	97	0.79 μM	2 μM		Y
Crizotinib		ALK (anaplastic lymphoma kinase) and ROS1 (c-ros oncogene 1) inhibitor	96			toxic	
Bosutinib		BCR-ABL and src tyrosine kinase inhibitor	96				

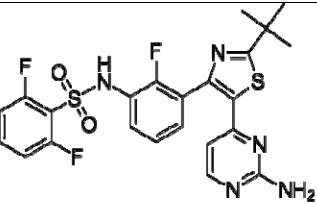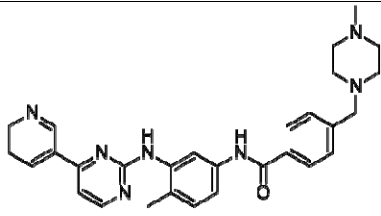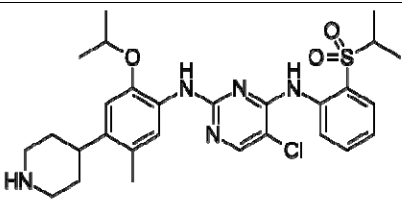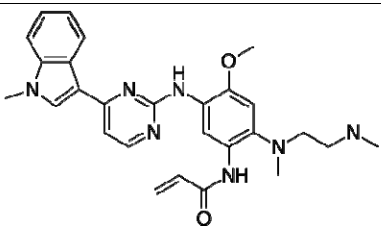|							
Axitinib		Its primary mechanism of action is thought to be vascular endothelial growth factor receptor 1-3, c-KIT and PDGFR inhibition	35	N			
Nilotinib		BCR-ABL and src tyrosine kinase inhibitor	66				
Dasatinib *Clinical trials Covid-19		BCR/Abl, Src, c-Kit, ephrin receptors, and several other tyrosine kinases	65	Y			
Linsitinib		Inhibitor of the insulin receptor and of the insulin-like growth factor 1 receptor	46				
Sorafenib		VEGFR, PDGFR and RAF kinases.	74				
Pazopanib		Multi target kinase inhibitor, vascular endothelial growth factor receptor (VEGFR), platelet-derived growth factor receptor (PDGFR), c-KIT and FGFR	20				
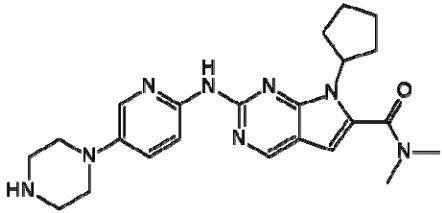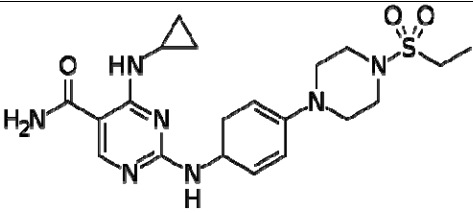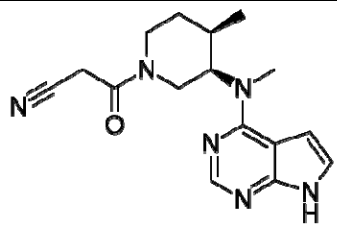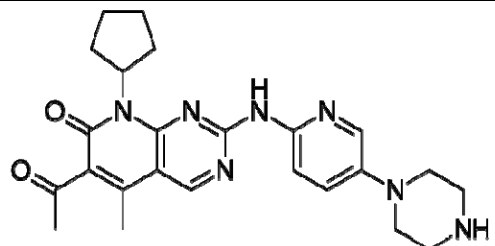
 Everolimus	Everolimus binds to its protein receptor FKBP12, which directly interacts with mTORC1, inhibiting its downstream signaling.	46				
 Midostaurin	Active against oncogenic CD135 (FMS-like tyrosine kinase 3 receptor, FLT3)	80				
 Sunitinib	Multi-targeted receptor tyrosine kinase (RTK) inhibitor. These include all receptors for platelet-derived growth factor (PDGF-Rs) and vascular endothelial growth factor receptors (VEGFRs),	96				
 Afatinib	Protein kinase inhibitor that also irreversibly inhibits human epidermal growth factor receptor 2 (Her2) and epidermal growth factor receptor (EGFR) kinases.	98	Y			
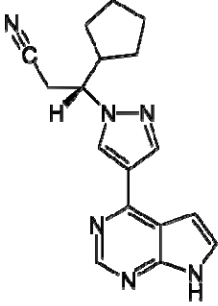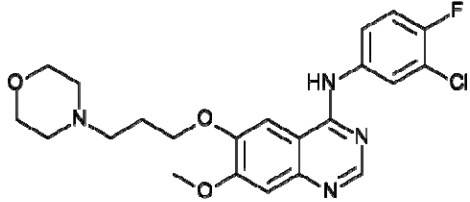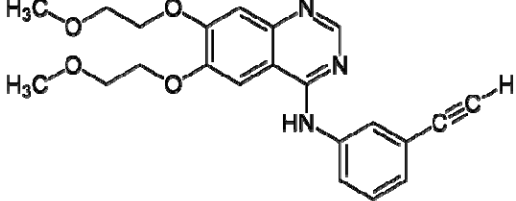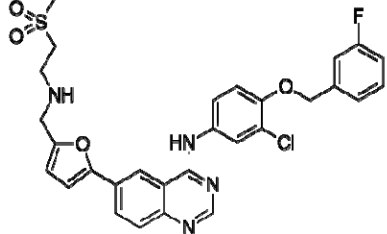
Name	Structure	Description	Value				
Regorafenib		Multi-kinase inhibitor, receptor tyrosine kinase (RTK.	65				
Rucaparib		enzyme poly ADP ribose polymerase (PARP).	-48				
Alisertib		Aurora A kinase inhibitor	19				
Tivozanib		VEGF receptor tyrosine kinase inhibitor	29				
Lenvatinib		Multiple kinase inhibitor against the VEGFR1, VEGFR2 and VEGF R3 kinases.	-12				
Ibrutinib *Clinical trials Covid-19		Bruton's tyrosine kinase(BTK)	-69				

Trametinib		MEK inhibitor	-40				
Ponatinib		Multi-targeted tyrosine-kinase inhibitor, primary BCR-ABL	98				
Vemurafenib		Inhibitor of the B-Raf enzyme , interrupts the B-Raf/MEK step on the B-Raf/MEK/ERK pathway – if the B-Raf has the common V600E mutation.	-3				
Defactinib		Inhibitor of FAK and PYK2	36				
Brigatinib		Anaplastic lymphoma kinase (ALK) and epidermal growth factor receptor (EGFR) inhibitor.	39	N			

Alectinib		Anaplastic lymphoma kinase (ALK)	62			
Cabozantinib		Tyrosine kinases c-Met and VEGFR2, and also inhibits AXL and RET.	61			
Idelalisib		Phosphoinositide 3-kinase inhibitor	17			
Cobimetinib		MEK inhibitor	82			
Galunisertib		TGF-β receptor type 1 kinase inhibitor	26			

Name	Structure	Description	Score				
Flumatinib		Inhibits the wild-type forms of Bcr-Abl, platelet-derived growth factor receptor (PDGFR) and mast/stem cell growth factor receptor (SCFR; c-Kit)	83				
Dabrafenib		Inhibitor of the associated enzyme B-Raf	-12				
Imatinib *Clinical trials Covid-19		Imatinib is specific for the *TK* domain in *abl* (the Abelson proto-oncogene), c-kit and PDGF-R (platelet-derived growth factor receptor).	81				
Ceritinib		Potent inhibitor of anaplastic lymphoma kinase (ALK)	94	Y			
Osimertinib		Third-generation epidermal growth factor receptor tyrosine kinase inhibitor.	98				

Ribociclib		Inhibitor of cyclin D1/CDK4 and CDK6	-4				
Cerdulatinib		SYK/JAK kinase inhibitor in development for treatment of hematological malignancies. It has lowest nM IC_{50} values against TYK2, JAK1, JAK2, JAK3, FMS, and SYK	78	N			
Tofacitinib *Clinical trials Covid-19		Inhibitor of the enzyme janus kinase 1 (JAK1) and janus kinase 3 (JAK 3)	-7				
Palbociclib		Selective inhibitor of the cyclin-dependent kinases CDK4 and CDK6	5				

Ruxolitinib *Clinical trials Covid-19		Janus kinase inhibitor (*JAK* inhibitor) with selectivity for subtypes JAK1 and JAK2	-46				
Gefitinib		Inhibitor of epidermal growth factor receptor's (EGFR) tyrosine kinase domain	81	Y			
Erlotinib		Inhibitor epidermal growth factor receptor (EGFR)	32				
Lapatinib		It is a dual tyrosine kinase inhibitor which interrupts the HER2/neu and epidermal growth factor receptor (EGFR) pathways	88				

Nintedanib *Clinical trials Covid-19		Competitively inhibits both nonreceptor tyrosine kinases (nRTKs) and receptor tyrosine kinases (RTKs). NRTK targets of nintedanib include Lck, Lyn, and Src. RTK targets of nintedanib include platelet-derived growth factor receptor (PDGFR) α and β; fibroblast growth factor receptor (FGFR) 1, 2, and 3; vascular endothelial growth factor receptor (VEGFR) 1, 2, and 3; and FLT3.	95				
Temsirolimus		Inhibitor of mTOR	4				

50

Supplemental References

1.   Premkumar, L. *et al.* The receptor binding domain of the viral spike protein is an immunodominant and highly specific target of antibodies in SARS-CoV-2 patients. *Sci Immunol* **5** (2020).

2.   Puhl, A.C. *et al.* Repurposing the Ebola and Marburg Virus Inhibitors Tilorone, Quinacrine, and Pyronaridine:. *ACS Omega* **6**, 7454-7468 (2021).

3.   Hou, Y.J. *et al.* SARS-CoV-2 Reverse Genetics Reveals a Variable Infection Gradient in the Respiratory Tract. *Cell* **182**, 429-446 e414 (2020).

4.   Yount, B., Denison, M.R., Weiss, S.R. & Baric, R.S. Systematic assembly of a full-length infectious cDNA of mouse hepatitis virus strain A59. *J Virol* **76**, 11065-11078 (2002).

5.   Spearman, C. The method of 'right and wrong cases' ('constant stimuli') without Gauss's formulae. *Brit J Psychol* **2**, 227-242 (1908).

6.   Kärber, G. Beitrag zur kollektiven behandlung pharmakologischer reihenversuche. *Archiv f Experiment Pathol u Pharmakol* **162**, 480-483 (1931).

7.   McCray, P.B. *et al.* Lethal infection of K18-hACE2 mice infected with severe acute respiratory syndrome coronavirus. *J Virol* **81**, 813-821 (2007).

8.   Oladunni, F.S. *et al.* Lethality of SARS-CoV-2 infection in K18 human angiotensin-converting enzyme 2 transgenic mice. *Nat Commun* **11**, 6122 (2020).

9.   Bao, L. *et al.* The pathogenicity of SARS-CoV-2 in hACE2 transgenic mice. *Nature* **583**, 830-833 (2020).

10. Yinda, C.K. *et al.* K18-hACE2 mice develop respiratory disease resembling severe COVID-19. *PLoS Pathog* **17**, e1009195 (2021).

11. Arce, V.M. & Costoya, J.A. SARS-CoV-2 infection in K18-ACE2 transgenic mice replicates human pulmonary disease in COVID-19. *Cell Mol Immunol* **18**, 513-514 (2021).

12. Moreau, G.B. *et al.* Evaluation of K18-. *Am J Trop Med Hyg* **103**, 1215-1219 (2020).

13. Winkler, E.S. *et al.* Publisher Correction: SARS-CoV-2 infection of human ACE2-transgenic mice causes severe lung inflammation and impaired function. *Nat Immunol* **21**, 1470 (2020).

14. Zheng, J. *et al.* COVID-19 treatments and pathogenesis including anosmia in K18-hACE2 mice. *Nature* **589**, 603-607 (2021).

15. Hsia, C.C., Hyde, D.M., Ochs, M., Weibel, E.R. & Structure, A.E.J.T.F.o.Q.A.o.L. An official research policy statement of the American Thoracic Society/European Respiratory Society: standards for quantitative assessment of lung structure. *Am J Respir Crit Care Med* **181**, 394-418 (2010).